Werk

Jahr: 1984
Kollektion: fid.geo
Signatur: 8 Z NAT 2148:54
Digitalisiert: Niedersächsische Staats- und Universitätsbibliothek Göttingen
Werk Id: PPN1015067948_0054
PURL: http://resolver.sub.uni-goettingen.de/purl?PPN1015067948_0054

LOG Id: LOG_0042
LOG Titel: Radiation belt particles and OII emissions determined as contaminations of geocoronal helium airglow observations
LOG Typ: article

Übergeordnetes Werk

Werk Id: PPN1015067948
PURL: http://resolver.sub.uni-goettingen.de/purl?PPN1015067948
OPAC: http://opac.sub.uni-goettingen.de/DB=1/PPN?PPN=1015067948

Contact

Niedersächsische Staats- und Universitätsbibliothek Göttingen
Georg-August-Universität Göttingen
Platz der Göttinger Sieben 1
37073 Göttingen
Germany
Email: gdz@sub.uni-goettingen.de

J Geophys (1984) 54:219-229

Journal of Geophysics

Radiation belt particles and OII emissions determined as contaminations of geocoronal Helium airglow observations

Hans J. Fahr and Günter Lay
Institut für Astrophysik und Extraterrestrische Forschung, Universität Bonn, Auf dem Hügel 71, 5300 Bonn 1, Federal Republic of Germany

Abstract. Four EUV absorption cell spectrophotometers were flown on board a Skylark 12 rocket in order to observe geocoronal and interplanetary HeI and HeII resonance line emissions. During this daytime rocket flight carried out from Natal (Brazil) up to an apogee of 830 km, in addition to HeI/HeII and OII emissions, specific non-electromagnetic contaminations of the count rates of the detectors were registered. These are shown here to be due to particle-induced events, most probably caused by middle-energetic electrons and/or protons.

The registered intensities are analyzed by fitting the raw observational data as a sum of different, theoretically suggested, contributions. As such, besides the particle-induced component, contributions from OII line emissions, from geocoronal and interplanetary HeI emissions and from plasmaspheric HeII emissions are discussed. Amongst the OII emissions taken into account, the only one of importance is shown to be that proportional to the O^+ ion column density on the line of sight of the detectors. This indicates that resonance scattering of O^+ ions most effectively contributes to the OII emissions in the height range above 400 km. The OII emission intensities decreasing with height according to a scale of about 200 km are the dominant contaminations below 500 km, whereas above 700 km these contaminations are negligible compared to those induced by particles. The OII emissions are found to contribute less than 10 percent to the integrated airglow intensity in the wavelength band between 500 and 800 Å, while more than 90 percent is due to HeI 537/584 Å emission.

The particle-induced component is independent of the viewing direction of the instrument but strongly dependent on height, with a steep increase in intensity above 600 km. This seems to confirm the existence of middle energetic electrons (2-11 keV) and/or protons (3-50 keV) in this height range at Natal.

Key words: EUV airglow - OII emissions - Radiation belt particles

Introduction

It has become evident in the past that the upper atmosphere of the earth is characterized by a large number of intense EUV resonance line emissions, mainly of HeI/II and OI/II. First observations of these emissions had been carried out using broadband airglow photometry by Meier and Weller (1972), Weller and Meier (1974), Paresce et al. (1973a), Ogawa and Tohmatsu (1971), Kumar et al. (1973) and Riegler and Garmire (1974). In a series of more recent publications Thomas and Anderson (1976), Gentieu et al. (1979), Anderson et al. (1980), Meier et al. (1980), Huffman et al. (1980), and Gentieu et al. (1981) have unequivocally documented, with their EUV-spectrometric results, that the upper atmosphere above 100 km is the source of a large multitude of resonance line emissions. The majority of these EUV airglow emissions is considered to be due to resonant scattering of solar EUV photos, to photoionization and to electron excitation processes involving He, O, N atoms and ions (Green and Barth, 1967; Dalgarno et al., 1969; Strickland and Donahue, 1970; Delaboundinière, 1977).

On the basis of their spectrometric EUV data in the height range between 100 and 300 km and in connection with theoretical model approaches, Feldman et al. (1981) recently carried out some interesting extrapolations to larger heights for some of the identified radiation components. The fact that some of these spectral contributions (for instance, OII-538 Å, OII-539/540 Å, HeI-537 Å, HeI-584 Å and OII-581 Å) cannot be separated due to limited spectral resolving powers, makes the extrapolations of these components questionable. In order to actually achieve a separation of these physically completely different components, the use of resonance absorption cell photometers is recommended, enabling a selective suppression of at least one of these components. In the rocket missions ASTRO-6 and ASTRO-HEL (Fahr et al., 1977; Lay et al., 1980) helium resonance absorption cells were used to suppress specifically the HeI-537/584 Å emissions. In the following we shall report on the analysis of the ASTRO-HEL absorption cell records which also revealed specific OII emission features and some non-electromagnetic, i.e. particle-induced, contributions to the registered intensities.

Offprints to: H.J. Fahr

Payload and mission description

The rocket payload ASTRO-HEL was aimed at the observation of geocoronal and interplanetary resonance emissions of neutral and ionized helium at HeI-584 Å

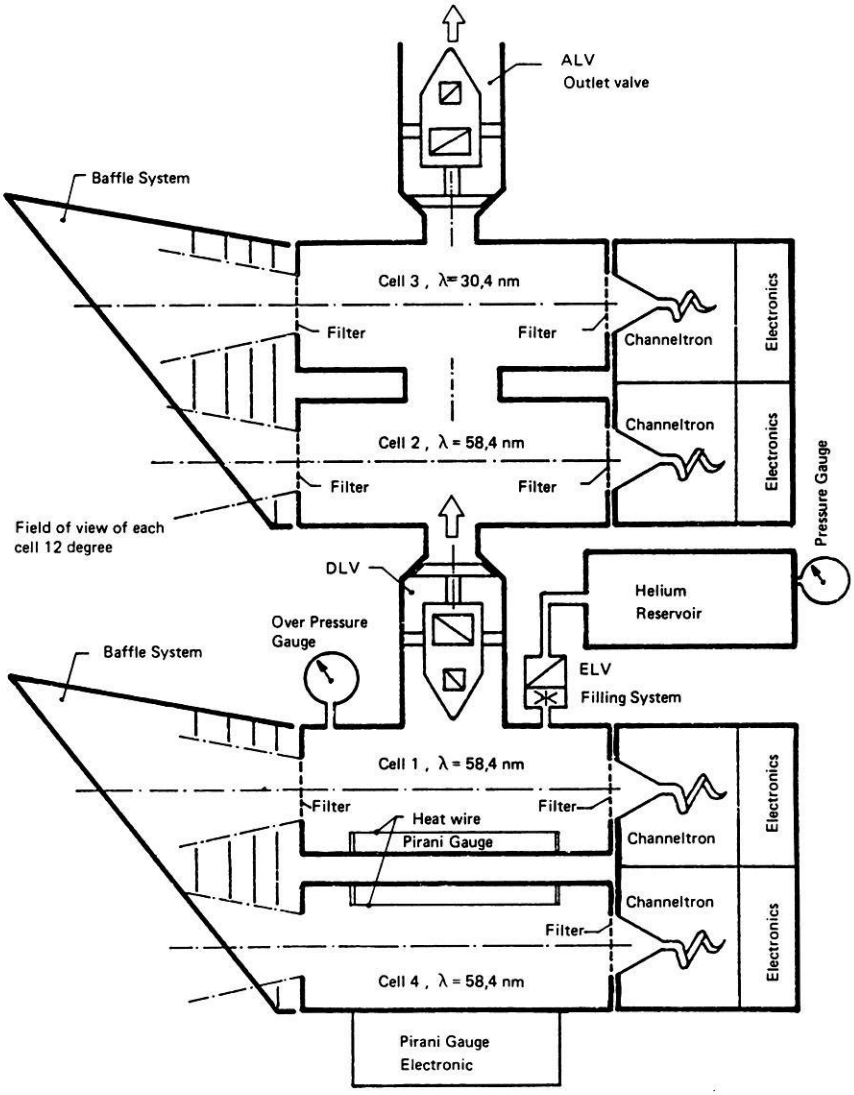

Fig. 1. General layout of the Astro-Hel experiment showing the four detectors D1 through D4, each consisting of a channeltron and an attached absorption cell individually equipped with front and rear filters

and HeII-304 Å. Detailled information concerning the origin and properties of these EUV emissions may be extracted from reviews by Thomas (1978) and Fahr and Shizgal (1983) and from references therein. For a reliable identification of the two spectrally different geocoronal and interplanetary emission components it was decided to use resonance absorption cell techniques (Maloy et al., 1978; Crifo et al., 1979; Lay et al., 1980).

The ASTRO-HEL payload consisted essentially of four EUV broadband photometers, three of which were combined with helium absorption cells. By the application of different gas pressures these cells could establish different helium column densities on the line of sight of the detectors and thus could reduce the intensities of those radiation components that either are in resonance with ground state helium atoms (HeI-537/584 Å) or could ionize the gas within the cells ($\lambda < 504$ Å).

Two of the four photometers (D1 and D2) intended as HeI-537/584 Å detectors had resonance cells closed with two, 2,000 Å thick, tin filters on their front and rear ends. The third photometer (D3) had a cell that was kept vacuum-tight by two aluminium-carbon filters and was used mainly as a HeII-304 Å detector. The fourth photometer (D4) served as a monitor of the integrated geocoronal HeI emissions and was equipped with an empty cell using only one tin filter in front of the photon detector. This empty cell was needed as a reference for the pressure-measuring device. The closed absorption cells (attached to D1, D2, D3) were built as an intercommunicating gas system that could be jointly evacuated and then filled up to specific helium gas pressures in a repeated manner. For the sake of a careful curve of growth analysis of the HeI emissions eight pressure levels (i.e. eight different He column densities) were programmed and used in flight. Figure 1 gives a general layout. A more detailed description of the payload is given by Lay et al. (1980).

The payload ASTRO-HEL was launched on 12 October 1979 at 11.09 LT (14.09 UT) from Natal (Brazil) with a three-stage Skylark 12 rocket. The apogee was reached at 830 km. During flight the common optical axis of the four coaligned photometers was successively pointed to nine celestial targets (marked in Fig. 2 with numbers 1 through 9), all located in the ecliptic plane. This pointing was selected to optimize the conditions for an observation of the upwind/downwind asymme-

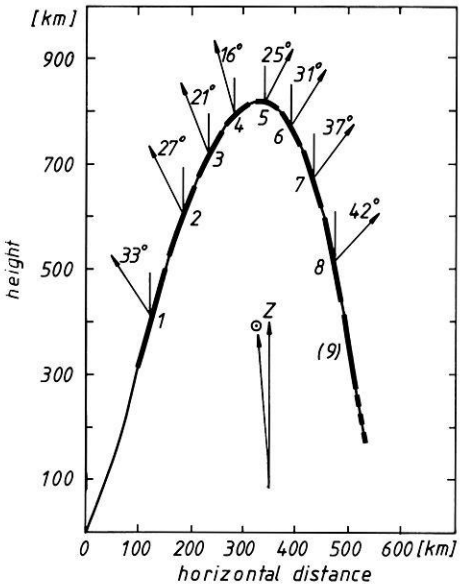

Fig. 2. The actual height of the payload is plotted versus horizontal distance from the launcher. The bold parts of the trajectory mark the position of the experiment while targets 1 through 9 are maintained with their respective local zenith angles of the line of sight. The directions to zenith (z) and sun ($\odot$) are indicated

tries of the interplanetary emission components. The line-of-sight vectors of these targets projected onto the orbital plane of the rocket are shown in Fig. 2. Each target was kept stable for 80 s. During this time period a full pressure cycle was run, which consisted of the consecutive realization of the eight programmed pressure levels distributed between 10 and 10^{-2} torr. The actual pressure in the absorption cells was monitored in flight by a Pirani gauge system, described in detail by Crifo et al. (1979). In Table 1 we have listed some relevant information on the payload and the mission. In Fig. 3 the complete data record registered in flight is shown.

Analysis of the Al-C photometer data: $\lambda < 500$ Å

First we shall study the EUV intensities registered by detector D3 equipped with an absorption cell closed at both ends by Al-C filters. Due to these broadband filters with a main transmission window between wavelengths of about 200–500 Å (see for instance Paresce et al., 1981), this detector was best suited for the observation of EUV radiation below 500 Å expected to be due to predominantly HeII-304 Å emissions from plasmaspheric helium ions. Since all of these radiation components with $\lambda < 500$ Å are able to ionize the neutral helium gas in the absorption cell, it was of interest to observe the pressure modulation of the integrated photon fluxes to obtain valuable information on the actual wavelengths.

In Fig. 4 we show an example of this modulation obtained during flight with the optical axis pointed to target no. 5. As one can notice there, though the registered intensities vary strongly with the helium pressures in the cell, substantial residual intensities still remain even at the highest pressure used in this cell, i.e. at 3.6 torr. This has implications for the nature of the radiation components registered by D3.

Table 1. Payload and mission data

Payload: Total weight: 134.3 kg

Four photometers (D1, D2, D3, D4), cone of acceptance 6° half angle; each consisting of channeltron (Spiraltron Galileo Optics CEM 4501)
+ absorption cell (length 12 cm, volume 151 cm^3)
+ two-stage baffle system

Specifically:

	Filter	Calibrated at wavelength	Transmission	CEM efficiency	Conversion factor [counts/s/Rayleigh]	Max. cell pressure
D1	2 × Sn	584 Å	5.6%	4.1%	15.7	10 torr
D2	2 × Sn	584 Å	3.8%	5.7%	14.8	3.6 torr
D3	2 × Al-C	304 Å	3.5%	6.7%	11.4	3.6 torr
D4	1 × Sn	584 Å	12.3%	4.8%	40.4	–

Thickness of filters: 2,000 Å

Bandpass of filters: Sn: 500–800 Å (10% of max. transmission)
Al-C: 150–550 Å (10% of max. transmission)

Absolute calibrations carried out with NBS-Al_2O_3 diode; accuracy 10%

Pressure measuring device: Pirani gauge system (2% error at maximum)

Cell temperature: 300 K

Mission:

Launch date:	Oct. 12, 1979 14.09 UT (11.09 LT)
Launch site:	Natal (Brazil); (6° S, 35° W; geogr./3.4° N, 34.7° E; geomag.)
Launcher settings:	84° EL, 289° AZ (ESE)
Apogee:	830 km
Observation period:	740 s (above 300 km)
Range of zenith angles:	16°–42°
Zurich number:	$R_Z = 189$
Solar flux:	$F_{10.7} = 216.4 \times 10^{-22}$ W m^{-2} Hz^{-1}
Magnetic indices:	$A_p = 8$; $K_p = 2$; $k_p = 3+$

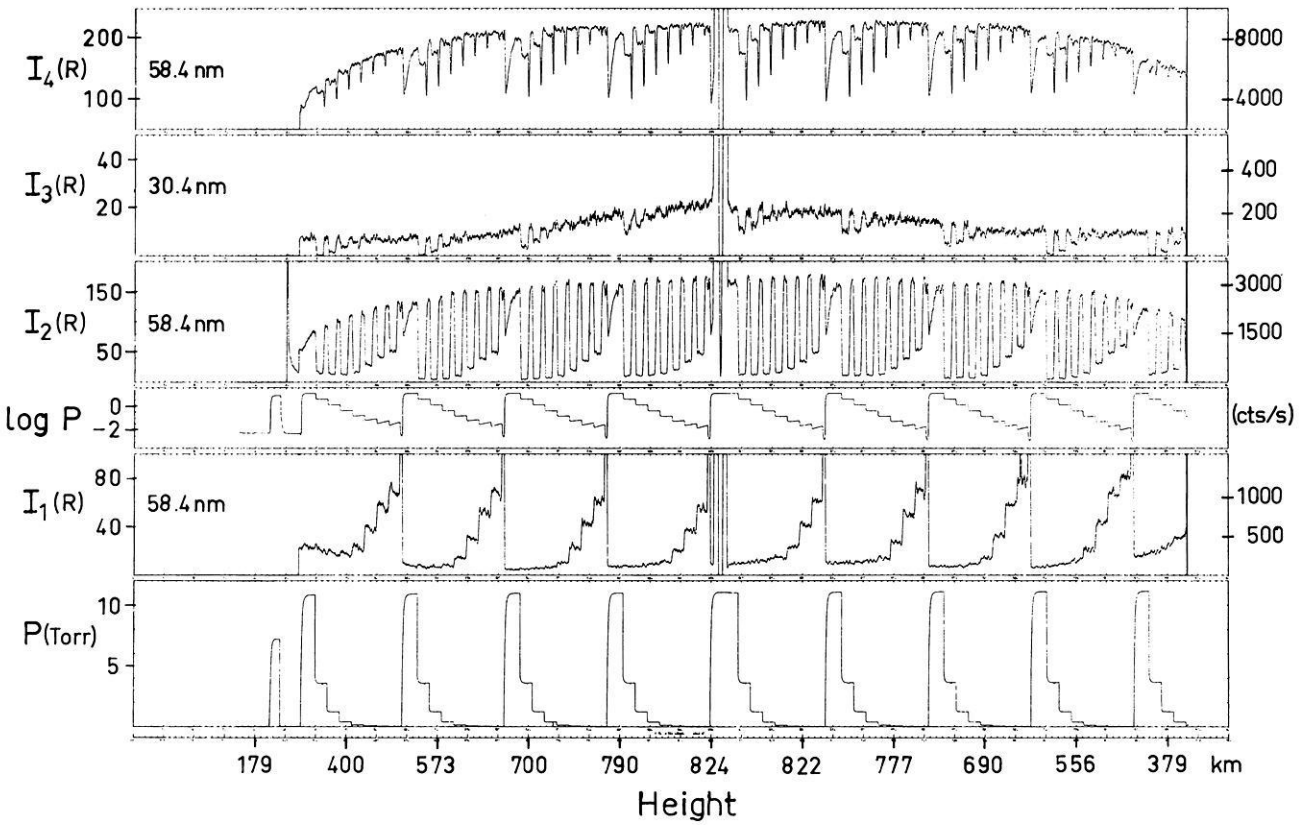

Fig. 3. The intensity data of detectors D1 through D4, together with the pressure in absorption cell 1, are shown versus height in km. The intensity scale in Rayleighs is valid only for the wavelengths indicated

It is evident that the remaining intensity $I_3(P_{max})$ cannot be due exclusively to HeII-304 Å radiation, as is seen in the following argument: The pressure modulation of a flux of photons with wavelength λ traversing an absorption cell with length L is given by the following general relation

$$I(P)=I(P=0)\cdot\exp\left[-n_{He}(P,T)\cdot L\cdot\sigma(\lambda)\right] \tag{1}$$

where $I(P)$ is the intensity registered at a helium pressure P in the cell, $n_{He}(P,T)$ is the helium density in the cell at pressure P and temperature T of the cell gas, and $\sigma(\lambda)$ is the cross section describing the extinction by helium atoms of photons with wavelength λ.

For HeII-304 Å photons the relevant extinction process is photoionization of helium characterized by a photoionization cross section $\sigma_i(304)=1.60\cdot10^{-18}\,\mathrm{cm}^2$ (Po Lee and Weissler, 1955). Thus, if the intensities I_3 registered by D3 at pressures $P=P_{max}=3.6$ torr and $P=0$ (empty cell) were due solely to 304 Å photons, the following ratio should be obtained:

$$\left.\frac{I_3(P=0)}{I_3(P_{max})}\right|_{theor.}=\exp\left[n_{He}(P_{max},T)\cdot L\cdot\sigma_i(304)\right]=9.27 \tag{2}$$

where the length L and temperature T have been inserted according to the numbers given in Table 1. However, only a ratio smaller than 2 is indicated in the data shown in Fig. 4. Furthermore, a small percentage of geocoronal HeI-537 Å radiation could in principle have been transmitted even by the Al-C filters and could have been seen by D3 (see Table 1). But due to the large relevant resonance absorption cross sections of helium gas for these resonance radiations ($\sigma_{res}=O(10^{-13}\,\mathrm{cm}^2)$), no contributions of the latter to the intensity $I_3(P_{max})$ are possible. In view of the maximum intensities of about 120 R seen by tin filter detectors D1 and D2 and the relative transmission at 584 Å of the Al-C filters compared to the tin filters of $Tr_{Al\text{-}C}/Tr_{Sn}=1.44\cdot10^{-2}$, a contribution of 1.8 R from HeI-584 Å to the empty cell intensity $I_3(P=0)$ (corresponding to about 10% of the total signal) could be expected at the most.

The subtraction of this fraction would leave an intensity ratio of

$$\left.\frac{0.9\cdot I_3(P=0)}{I_3(P_{max})}\right|_{obs}=1.8=\exp\left[(n_{He}(P_{max},T)\cdot L\cdot\sigma_{eff}\right]=Tr_{He}(\lambda_{eff}) \tag{3}$$

to be explained as due to the absorption of the helium gas in the absorption cell according to an effective cross section σ_{eff}. The results shown in Fig. 4 would thus require an effective cross section of $\sigma_{eff}=4.2\cdot10^{-19}\,\mathrm{cm}^2$. If photons shortwards of 504 Å (photoionizing helium) are taken as responsible for the D3 signal, this would imply an effective wavelength of $\lambda_{eff}=195$ Å. However, airglow photon fluxes of such small wavelengths with intensities causing a signal of 170 counts/s at D3 have never been reported in the literature. Thus this explanation is ruled out. In prin-

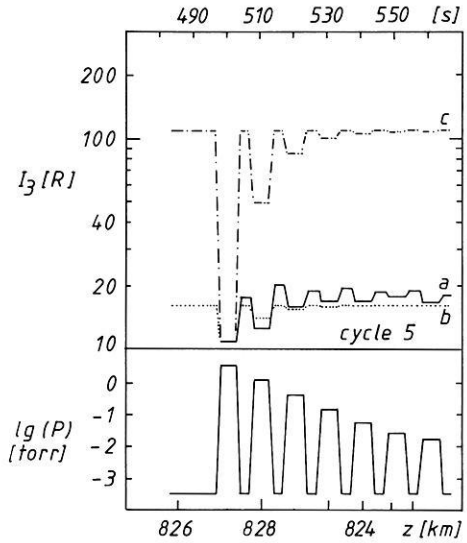

Fig. 4. The D3 intensity data (in Rayleighs) for target no. 5 are plotted versus height (time after launch) in the *upper panel* (curve *a*) and the respective He gas pressure in the absorption cell in the *lower panel*. Curve *b* gives the best fit to the data according to Eq. (1) with $\sigma_{eff} = 2.9 \cdot 10^{-19}$ cm^2. Curve *c* was calculated with the photoionization cross section $\sigma_i(304) = 1.6 \cdot 10^{18}$ cm^2 (Po Lee and Weissler, 1955) bound to the measured intensity at the highest pressure. (Here the Rayleigh units are valid only for a 304 Å photon signal; otherwise the conversion factor given in Table 1 has to be applied)

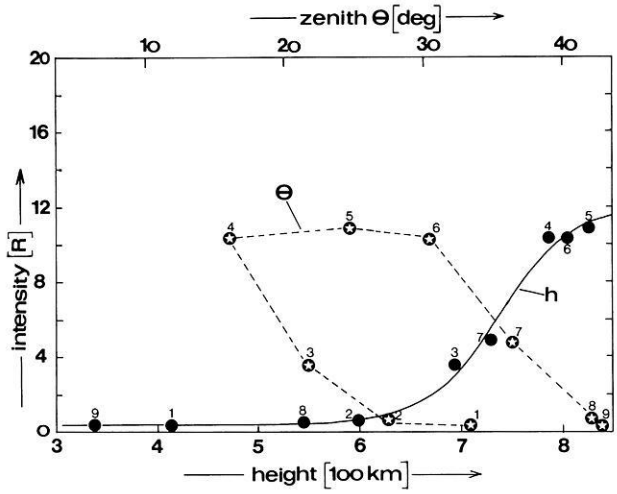

Fig. 5. The D3 intensities $I_3(P_{max})$ for targets 1 through 9 are plotted versus height of observation (*full circles*) and versus zenith angle θ of the line of sight (*asterisks*). The *solid line* represents a best fit to the data according to the last term in Eq. (4). (See caption of Fig. 4 concerning the units of Rayleighs)

ciple also photons longwards of 504 Å could lead to the observed signal ratios if they were resonantly scattered by neutral helium atoms. In this context, only OII-538 Å airglow photons come into question. Due to their distance of 0.8 Å from the HeI-537 Å resonance line, they could in principle also resonate with ground state helium atoms according to an absorption cross section of $5 \cdot 10^{-21}$ cm^2, which is not of the required order of magnitude. In addition, the fact that according to Gentieu et al. (1979) and Feldman et al. (1981) the OII-538 Å emissions strongly decrease with height, whereas the measured intensities $I_3(P_{max})$ increase with height, also rules out these intensities as a major fraction of the signal.

Summarizing, we can thus state that at the highest pressure $P_{max} = 3.6$ torr realized in the absorption cell of D3 no contributions to $I_3(P_{max})$ from either HeI-584 Å or HeI-537 Å radiation and nearly no contributions from HeII-304 Å radiation must be expected. Rather, these intensities must be taken as due to:

1) photon fluxes at wavelengths $\lambda > 504$ Å which are unable either to resonate with helium atoms or to ionize them. This is caused by either OII airglow emissions or by solar EUV stray light that originates at the illuminated parts of the outer edges of the baffle system in front of the sensors, or due to:

2) a particle flux, which either penetrates the filters and hits the active channeltron detector surface or impinges upon the filters and releases there EUV photons that are counted by the detector, or which has direct access to the channeltron detector.

We have attempted to fit the high pressure intensity data of D3 as a sum of those contributions left over in the previous discussion. In order to obtain first a rough idea for the appropriate theoretical representation of these contributions contained in the registrations $I_3(P_{max})$ they have been plotted in Fig. 5 versus both height of observation and zenith angle θ of the line of sight. Figure 5 manifests that the data $I_3(P_{max})$ predominantly contain a component that is closely correlated with height, whereas no correlation with the zenith angle is indicated.

This means that only a minor part of the signals can be due to contributions from OII airglow emissions which above 400 km are represented by an optically thin radiation field with pronounced dependencies of the intensities on the viewing direction. Also, contributions from solar stray light contaminations that should be characterized by distinct correlations with the viewing direction can be excluded as the major part of the signals.

In contrast, one must conclude that a predominant part of the signals is due to a component exclusively dependent on height with a steep intensity increase from heights of around 500 km upwards towards the apogee. The height-dependence of this component is shown by the continuous curve drawn in Fig. 5.

In order to perform a numerical best-fit procedure for the data at highest pressure P_{max} one has to take into account in principle four different physical contributions, namely:

1) solar EUV stray-light contamination

2) OII line emissions due to solar photoionization of atmospheric O atoms (ionization into an excited state)

3) scattering of solar EUV resonance line photons at atmospheric O^+ ions (most probable emissions: 539/540/581 Å)

4) a radiation component exclusively height-dependent with a height profile extracted from Fig. 5.

With these contributions we arrive at the following general representation for the data obtained under P_{max}:

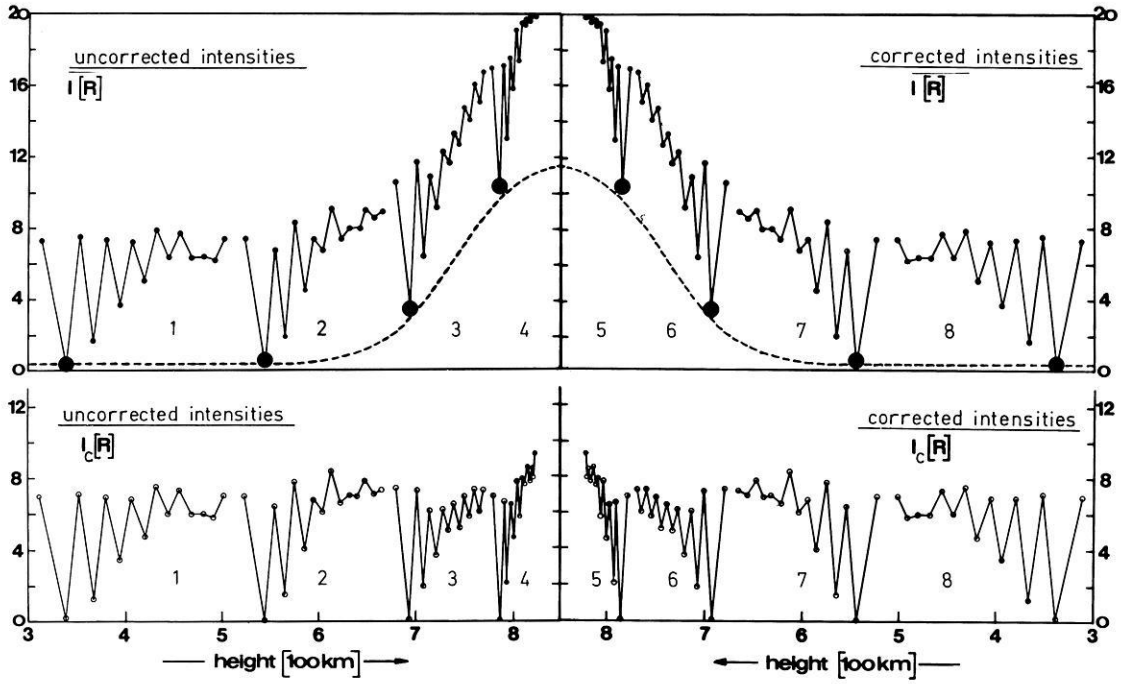

Fig. 6. The *upper panel* shows the registered intensities I_3 versus height for targets 1 through 8. The *full circles* mark the intensities $I_3(P_{max})$ used in Fig. 5. Subtraction of the height-dependent correction function given by the *broken line* yields the data plotted in the *lower panel*. The "saw tooth" shape is due to the varying pressure in the absorption cell. (See caption of Fig. 4 concerning the unit of Rayleighs.)

$$I(P_{max}) = \frac{C_1}{\sin^2\gamma} + \frac{C_2}{\cos\theta}\cdot\exp(-h/H_{OI}) + \frac{C_3}{\cos\theta}\cdot\exp(-h/H_{OII}) + C_4\cdot\left(\frac{1}{1+\beta}+\frac{C_5}{1+1/\beta}\right) \quad (4)$$

where β has the following form:

$$\beta = \exp[(h-C_6)/C_7] \quad (5)$$

with h measured in km.

The theoretical representations of components 1) through 4) are motivated in the following ways:

1) According to Leinert and Klüppelberg (1974) and Landau and Lifshitz (1964) the intensities diffracted by an illuminated edge of the baffle system of the instruments is proportional to $(1/\sin^2 g)$ where g is the diffraction angle of the incidental light ray. This dependence of the stray light intensity on the diffraction angle is valid over the whole electromagnetic spectrum, as was already shown by Sommerfeld in 1894 (Sommerfeld, 1896). As justified by the small aperture of our instruments (see Table 1), we have taken the angle between the optical axis and the direction to the sun as a mean diffraction angle necessary for solar stray light photons to enter the photometers. The quantity C_1 contains the integral $\int \lambda\cdot F_{sol}(\lambda)\, Tr_{Al\text{-}C}(\lambda)\, Tr_{He}(\lambda) d\lambda$ carried out over the bandpass of the detectors in question. At heights above 300 km and at a constant pressure P_{max} this integral represents a constant for all observations, as well as C_1 itself.

2) Due to the low ionization cross section for the photoionization of O atoms by solar EUV photons, the solar EUV photon flux at heights above 300 km can be taken as constant. Thus the source function for this OII emission is simply proportional to the local OI density, i.e. the total intensity is proportional to the OI column density on the line of sight due to the optically thin nature of this radiation field. The representation given in Eq. (4) uses a constant OI density scale height H_{OI}.

3) Due to the optically thin radiation field of resonantly scattered solar photons, the intensity is proportional to the column density of the scatters, i.e. of O^+ ions, and with a constant scale height H_{OII} the third term in Eq. (4) is obtained.

4) The form of the height-dependence of the fourth term was suggested by the curve given in Fig. 5.

In the application of formula (4) to the $I_3(P_{max})$ data one can take $C_2 = C_3 = 0$ due to the transmissivity properties of the Al-C filters. In the framework of the fit procedure the values of the remaining constants are then obtained as:

$$C_1 = 3\cdot 10^{-3}, \quad C_4 = 0.4, \quad C_5 = 30.25, \quad C_6 = 740, \quad C_7 = 36.5$$

yielding a satisfactory representation of the data within the limits of uncertainty of the instruments. These numbers reveal that solar stray light contaminations can be neglected, proving the quality of the baffle system.

The result of this fit is shown in Fig. 6. In the upper half of this figure the uncorrected signals of detector D3 taken at targets 1 through 8 are plotted versus height. In the lower half the best fit values for the "high pressure" intensities $I_3(P_{max})$ have been subtracted from the original data of D3. The reduced intensities $I_{3,c} = I_3(P) - I_3(P_{max})$ solely containing pressure-modulated intensity components reveal fairly small variations with target number.

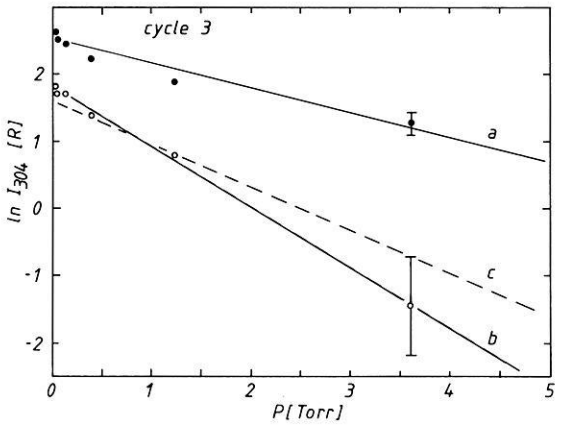

Fig. 7. Detector D3 data for target no 3 are plotted versus the gas pressure in the absorption cell: 1) registered intensities $I_3(P)$ (*full circles*) and best fit line *a*; 2) corrected intensities $I_{3,c}(P)$ (*open circles*) and best fit line *b*. The slope of lines *a* and *b* yields an effective cross section of $9.5 \cdot 10^{-19}$ cm^2 and $2.33 \cdot 10^{-18}$ cm^2, respectively, while the *broken line c* corresponds to the photoionization cross section $\sigma_i = 1.6 \cdot 10^{-18}$ cm^2 (Po Lee and Weissler, 1955). Error bars are given at 3.6 Torr. (See caption of Fig. 4 concerning the use of Rayleigh units)

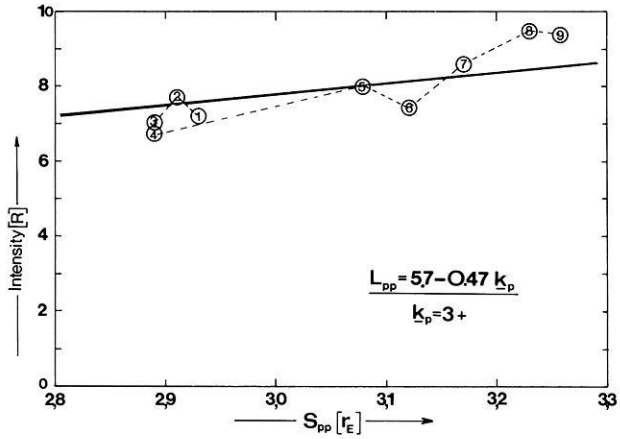

Fig. 8. This is a plot of the reduced intensity $I_{3,c}$ extrapolated towards $P=0$ Torr for targets 1 through 9 versus the length S_{pp} of the line of sight within the plasmasphere. In calculating S_{pp} the given Binsack formula was used with the actual value $k_p = 3+$. The straight line gives the best fit to the data

The fact that these intensities $I_{3,c}$ mainly contain contributions from HeII-304 Å emission is manifest from Fig. 7, where we have plotted for one pressure cycle the logarithm of $I_{3,c}$ versus the pressure P in the helium cell. The theoretical expectations derived from a pressure modulation according to Eq. (1) are nearly fulfilled, which obviously does not hold for the unreduced intensities $I_3(P)$ also plotted in Fig. 7. The effective cross section σ_{eff} best fitting the reduced intensities is somewhat larger than the well-known value for σ_i (304) $= 1.60 \cdot 10^{-18}$ cm^2. This must be taken as an indication for minor contributions from HeI emission to $I_{3,c}(P=0)$.

Additional support for the suspicion that the reduced intensities $I_{3,c}$ predominantly contain contributions from 304 Å emission may also be taken from the results presented in Fig. 8. Assuming that the geocoronal emission at 304 Å seen from heights above 400 km is due to solar HeII-304 Å photons resonantly scattered at plasmaspheric He^+ ions (which is true to a very high degree of accuracy), one can easily arrive at a reasonably good estimate for this emission. As a first order approximation a constant plasmaspheric density n_{He^+} and a temperature T_{He^+} can be used, as suggested by the plasmaspheric model by Chiu et al. (1979). With this and the optically thin conditions prevalent for the plasmaspheric HeII-304 Å emission one obtains the relation

$$I_{304}(\mathbf{r}, \mathbb{Q}) = A \cdot S_{pp}(\mathbf{r}, \mathbb{Q}) \tag{6}$$

where A is a constant containing relevant atomic quantities, the solar flux at 304 Å and the average helium density and temperature n_{He^+} and T_{He^+}, respectively. The quantity S_{pp} is the length of the line of sight within the plasmasphere starting from an observer at $\mathbf{r}$ and pointed to a direction $\mathbb{Q}$.

The plasmapause on the earth's dayside is given to a very good approximation by the outermost closed magnetic dipole field line that belongs to an L-shell value L_{pp}. According to an improved Binsack formula proposed by Carpenter and Park (1973), an appropriate value for L_{pp} in units of earth radii R_E is proportional to index k_p, which is the maximum value of the geomagnetic activity index K_p during the 12-hour period preceding the time of observation. For our conditions k_p is 3+ and hence leads to L_{pp}:

$$L_{pp} = 5.7 - 0.47\, k_p = 4.15 \quad [R_E]. \tag{7}$$

Since for each of our targets i the viewing direction $\mathbb{Q}_i$ is known, the length $S_{pp,i}$ of the line of sight inside the plasmasphere can be evaluated if a standard geomagnetic dipole field model is used.

In Fig. 8 we have plotted the reduced intensities $I_{3,c}(P=0)$ versus corresponding plasmapause distances S_{pp}. A fairly good correlation to a straight line, representing the expected proportionality according to Eq. (6), is reached. This may be taken as further confirmation for the fact that the obtained data $I_{3,c}$ predominantly contain contributions from plasmaspheric HeII-304 Å emission. Based on an integrated solar line flux at 304 Å of $[\pi \cdot F_{sol}(304)] = 9 \cdot 10^9$ phot/cm^{2}s as extrapolated for our actual 10.7 cm flux value from a curve given in Heroux and Higgins (1977) and a solar line width of 0.15 Å (Behring et al., 1972), we derive with the formula given in Chakrabarti et al. (1982) from Fig. 8 an average plasmaspheric He^+ density value of $n_{He^+} = 2 \cdot 10^2$ cm^{-3}. This compares well with values quoted by other authors (for instance, Paresce et al., 1973b).

Analysis of the Sn-photometer data: $\lambda > 500$ Å

Detectors D1 and D2 equipped with two tin filters were intended for the observation of geocoronal HeI-584 Å emission. The data obtained with these detectors reveals, however, that other emissions have also been registered during the flight. This is especially evident in the records of detector D1 obtained under a helium pressure of 10 torr.

Transmissivity calculations prove that under such helium pressures no contributions from emissions res-

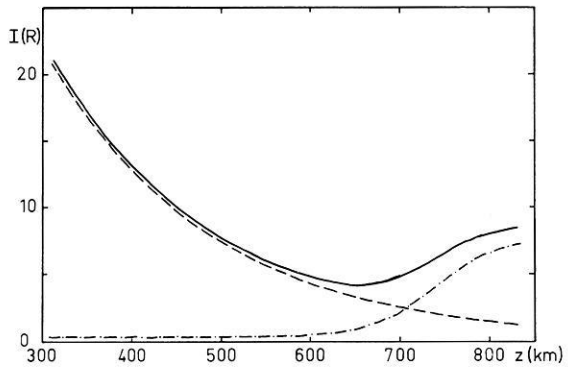

Fig. 9. The contaminating intensities inherent in the D1 data (*solid line*) are shown as a function of height as determined according to Eq. (4). This contaminating signal consists of OII-line emissions (*broken line:* zenith conditions!) and a particle-induced contribution (*dashed-dotted curve*). For the unit [counts/s] use the conversion factor listed in Table 1

onantly scattered by neutral helium atoms can be contained in the signal, i.e. the data $I_1(P_{max})$ are free from HeI-584/537 Å contributions. At a helium pressure of 10 torr the absorption cell has an optical thickness τ much larger than 1 ($\tau \simeq 10^5$) both for HeI-584 Å and HeI-537 Å photons. However, it has been proven that the "single scatter" transmissivity (which is very small in this case) is increased by multiply scattered photons by only a negligibly small fraction (Delaboudinière, 1979). Due to the "single scatter" absorption profile of the cell at 10 torr it is thus also ascertained that even interplanetary photons are completely suppressed.

For an interpretation of these $I_1(P_{max})$ data we shall again make use of Eq. (4). There is no doubt that contributions according to terms 1 through 3 in that equation have to be expected in data channel D1 (and D2), but the fourth requires some more arguing. Since within the bandpasses of our instruments, except for the case of HeI-584 Å, no optically thick radiation fields are present above 500 km, the height dependence of this term by no means can be explained by photons, leaving only the possibility of a count rate caused by particles. Such particle events would show up in all detectors with the same height profile but, maybe, with a different magnitude. For the fitting procedure we thus took the same coefficients C_5, C_6 and C_7 as found from the I_3 data in the previous section.

The result of this fit procedure is presented in Fig. 9 which displays versus height the fitted intensities $I_1(P_{max})$ for zenith observational conditions. The dashed lines indicate the two principally different contributions to these intensities, namely electromagnetic contributions (curve decreasing with height) and particle-induced contributions (curve increasing with height). Again here, a satisfactory representation of the data within the experiment's limits of accuracy was reached with the following values for the constants C_1 through C_4 in Formula (4):

$$C_1 = 1.7 \cdot 10^{-7}, \quad C_2 = 0.2, \quad C_3 = 85.7, \quad C_4 = 0.26.$$

An identical procedure was applied to the D2 data, yielding the same results. For this fit an OI scale height $H_{OI} = 85$ km derived from the MSIS atmospheric model (Hedin et al., 1977a/b) was used. The OII scale height representing an average quantity characteristic for the region of contributing OII emitters was also subject to the fit procedure and was obtained with a value $H_{OII} = 215$ km, in reasonably good accordance with the ionospheric IRI model (Rawer et al., 1978). With the value obtained for C_1 again the quality of the baffle system is also proven for these detectors (D1 and D2). i.e. essentially no solar stray light is contaminating our data.

Furthermore, it can be concluded that also contributions from the second term in Formula (4), i.e. the ionization of OI into an excited state, are negligible in the relevant height range. The only contributing terms are due to OII-induced emissions and particle events, both of which shall be discussed in the next section.

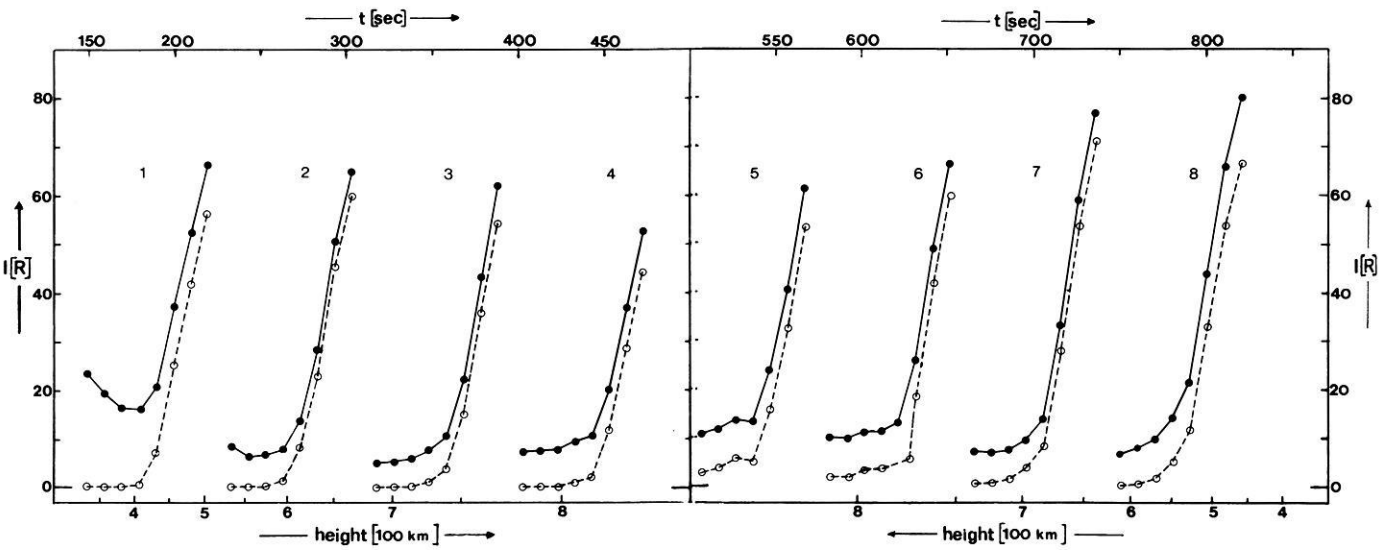

Fig. 10. The I_1 intensity (584 Å data) for targets 1 through 8 are shown versus height and time after launch. The full circles represent the registered data. Subtraction of the correction function given in Fig. 9 yields the *open circles (dashed curves)*. The intensity increase within each cycle is correlated with the decreasing pressure in the absorption cell. Here the Rayleigh units are valid only for a 584 Å photon signal. Otherwise, the conversion factor given in Table 1 has to be applied

If again the "high pressure" intensities $I_1(P_{max})$ obtained in the fit procedure are subtracted from the D1 registrations, one arrives at the following result for the reduced intensities $I_{1,c}(P)=I_1(P)-I_1(P_{max})$ shown in Fig. 10. The full circles give the original data registered under different pressures at different targets, whereas the open circles show the corresponding reduced intensities $I_{1,c}$.

These reduced intensities, in contrast to the original data, can now be represented by HeI-584 Å radiation profiles due to geocoronal and interplanetary resonance radiation transmitted through the absorption cell of the experiment. This will be discussed in more detail in a forthcoming paper.

Conclusions

Electromagnetic component

The analysis of the D3 data showed that no OII emissions at wavelengths smaller than 500 Å are present. On the other hand, the analysis of the D1 data confirms the presence of OII emissions in the wavelength band between 500 and 800 Å. These emissions are shown to be exclusively connected with directly excited O^+ ions and not to be caused by ionizations of O atoms into an excited state, at least not at heights above 300 km for near-zenith observations at local noon and low geomagnetic latitudes. This shows that amongst the processes under discussion as responsible for OII airglow emissions (Dalgarno et al., 1969; Delaboudinière, 1977; Feldman et al., 1981), the one connected with O atoms is negligible for our circumstances.

In contrast, OII intensities proportional to the OII column density are confirmed. The average O^+ ion scale height used in our quasi-barometric OII density representation was best fitted by a value of $H_{OII}=215$ km.

At heights below 600 km these OII emissions are the dominant contribution to the $I_{1,c}(P_{max})$ data. They reach up to 25% of the HeI airglow emissions registered by detectors D1/D2. Under daytime conditions near the geomagnetic equator, OII emissions above 300 km thus do not contribute more than 25% to the total signal registered in a broadband photometer channel at wavelengths between 500–800 Å. This probably also permits the conclusion that in the spectrometer peaks at around 540 Å and 580 Å registered with the STP-78-1 EUV spectrometer device (Chakrabarti et al., 1983) the major contributions originate from HeI 537/584 Å emissions rather than from OII emissions.

Particle-induced component

This component is characterized by a steep increase with height above 600 km and by an independence of the viewing direction. These properties point to magnetically controlled particles, namely electrons or protons of the inner radiation belt. These particles can be counted by the channeltrons either after approaching the instrument within the optical cone of acceptance and traversing the filters of the absorption cell or after direct access. In the latter case, particles can be considered either as practically unaffected by the surrounding material due to their high energies or are moderated by this material. Due to the different material environments of the detectors in the payload the moderation case can be ruled out since it would lead to different count rates at all detectors, which is not true for the count rates of detectors D1 and D2. The unmoderated high energy case, on the other hand, would require identical count rates at all detectors, which is not true for detectors D3 and D1, D2. Thus the only explanation for the particle-induced component is given by particles that reach the channeltrons after traversal of the cell filters. The different count rates at D3 and D1 (D2) respectively, are then explained by the different filter materials. The release of photons in either of the filters is considered to be unlikely.

The appearance of such energetic belt particles at heights around 500 km during our rocket flight was very likely since the launch took place at Natal, Brazil, i.e. at the periphery of the South Atlantic anomaly. Due to "high energy" background radiation in this region, information on the fluxes and spectra of belt particles is rather poor and of a low degree of accuracy. For instance, no values for the energy range below 30 keV could be found in the literature until 1981 (Gledhill and Hoffman, 1981). From their Atmosphere Explorer C data taken in the region of the South Atlantic anomaly at heights close to 300 km electron spectra are obtained which can be represented by a power law in the energy range between 0.2–26 keV, with a spectral index close to $\gamma=-1$.

A power law has also been confirmed at higher particle energies for electrons, e.g. by Burrows and McDiarmid (1972), and for protons by Vernov et al. (1967).

The relevant energy range of the particles counted by our instrument is found by the following reasoning: for detectors D1 and D4 which are equipped with one and two tin filters, respectively, we can define minimum energies E_c required for electrons or protons to penetrate these metal filters, all having a thickness of about 2,000 Å. Therefore, these minimum energies for detectors D1 and D4 derived from the "energy-range" relation (Landolt-Börnstein, 1952; Marion, 1972) can be calculated and are given in Table 2.

From Table 2 it can be learned that the particle-induced signal is due to particles with energies larger than E_c, i.e. for instance in detector D1 electrons (protons) with energies larger than 5 (12) keV could have been seen. Thus in connection with a power law, particles with energies E close to or slightly larger than E_c are most likely to be responsible for our count rates. Using a power law, we attempt to represent the registered particle fluxes ϕ by:

$$\phi=\psi_0 \int_{E_c}^{\infty} \left(\frac{E}{E_0}\right)^{-\gamma} dE \tag{8}$$

where ψ_0 is the differential particle flux at an energy E_0 and γ is the actual spectral index. In this relation we have to assume that all particles with energies $E>E_c$ that penetrate the filters are registered with identical efficiency by the channeltrons. With (8) we can obtain the value for γ from:

$$\gamma=1-\frac{\ln\phi_4-\ln\phi_1}{\ln E_{c_4}-\ln E_{c_1}}. \tag{9}$$

Table 2

Detector	Minimum Energies		ϕ [counts s^{-1} cm^{-2} sr^{-1}]
	Electrons E_c [keV]	Protons E_c [keV]	
D1, D2 (2 Sn filters ≙4,000 Å Sn)	5	12	$\phi_1 = 1{,}280$
D3 (2 Al-C filters ≙4,000 Å Al-C)	4	11.4	$\phi_3 = 1{,}590$
D4 (1 Sn filter ≙2,000 Å Sn)	2.5	3.4	$\phi_4 = 9{,}900$

ϕ = total particle-induced contamination registered by detectors D1 through D4 at 800 km

Taking the values listed in Table 2, one arrives at a spectral index $\gamma_e = 3.95$ for electrons or $\gamma_p = 2.62$ for protons if the registered fluxes ϕ are taken as due to electrons or protons only.

The differential flux values $\psi_0(e)$, $\psi_0(p)$ for electrons and protons then are:

$$\psi_0(e) = 4.36 \cdot 10^5 \ [\mathrm{cm^{-2}\ s^{-1}\ sr^{-1}\ keV^{-1}}], \quad (10)$$

$$\psi_0(p) = 1.16 \cdot 10^5 \ [\mathrm{cm^{-2}\ s^{-1}\ sr^{-1}\ keV^{-1}})] \quad (11)$$

at a reference energy $E_0 = 1$ keV and a channeltron efficiency of 100%.

In view of the very low proton fluxes found by Gledhill and Hoffman (1981) in this low energy range at heights around 300 km and in view of higher deflection angles and lower counting chances for protons, proton fluxes are unlikely to be responsible for our particle-induced signal. Therefore we are left with electrons to cause our count rates ϕ. For the electron flux we have derived the following power law:

$$\phi(e) = 4.36 \cdot 10^5 \ (E/E_0)^{-3.95} \ [\mathrm{cm^{-2}\ s^{-1}\ keV^{-1}}]. \quad (12)$$

At first glance, the high values obtained for both the spectral index and the differential flux value at 1 keV do not seem to be in accordance with the results of Gledhill and Hoffman. However, the following deviating conditions have to be carefully taken into account. For the electrons we have a minimum energy requirement of $E_c = 5$ keV, whereas the energy cut-off in the instrument of Gledhill and Hoffman is much lower, i.e. $E_c = 0.2$ keV.

Taking the spectrum of Gledhill and Hoffman obtained for a K_p-value that is comparable to our conditions, we can recognize that this spectrum reveals a steepening for energies upwards of 5 keV, suggesting both a higher spectral index $\gamma > 1.15$ and a higher extrapolated spectral flux $\psi_0(e)$ at 1 keV.

Furthermore, the difference in height between our observations and those of Gledhill and Hoffman has to be considered. A specific power law distribution of electron energies at 800 km tends to flatten out at lower heights due to the selective depletion of low energy electrons that are reflected upwards at their relatively high mirror points.

Regarding the relatively high fluxes $\psi_0(e)$ at 800 km that we have derived, we can draw the attention to the height profiles found for ϕ. As is shown in Figs. 6 and 9, a decrease in the fluxes by a factor of at least 20 is indicated for a decrease in height from 800 down to 300 km. In view of these arguments, our results do not contrast with those of Gledhill and Hoffman.

Finally, we can justify our assumption that the particle-induced signal is unaffected by the helium gas target in the cells since it can be shown that the particles responsible, i.e. electrons with energies $E > E_c = 5$ keV, are unmodulated by the helium gas columns in our cells even at the highest pressures used. This can be deduced from the application of the energy-range relation to electrons in helium gas targets (Marion, 1972).

References

Anderson, Jr., D.E., Feldman, P.D., Gentieu, E.P., Meier, R.R.: The UV dayglow 2, Ly α and Ly β emissions and the H distribution in the mesosphere and thermosphere. Geophys. Res. Lett. **7**, 529–532, 1980

Behring, W.E., Cohen, L., Feldman, U.: The solar spectrum: wavelengths and identifications from 60 to 385 Angstroms. Ap J. **175**, 493–523, 1972

Burrows, J.R., McDiarmid, I.B.: Trapped particle boundary regions. Proc. COSPAR, IAGA, URSI Symp. on "Critical Problems of Magnetospheric Physics", Madrid (Spain), 83–104, 1972

Carpenter, D.L., Park, C.G.: On what ionospheric workers should known about the plasmapause-plasmasphere. Rev. Geophys. Space Phys. **11**, 133–154, 1973

Chakrabarti, S., Paresce, F., Bowyer, S., Chiu, Y.T., Aikin, A.: Plasmaspheric helium ion distribution from satellite observations of the HeII 304 Å. Geophys. Res. Lett., **9**, 151–154, 1982

Chakrabarti, S., Paresce, F., Bowyer, S., Kimble, R., Kumar, S.: The extreme ultraviolet day airglow. J. Geophys. Res., **88**, 4898–4904, 1983

Chiu, Y.T., Luhmann, J.G., Ching, B.K., Boucher, Jr., D.J.: An equilibrium model of plasmaspheric composition and density. J. Geophys. Res. **84**, 909–916, 1979

Crifo, J.F., Fahr, H.J., Seidl, P., Wulf-Mathies, C.: Rocket-borne instrumentation using the resonant absorption technique to study the geocoronal and interplanetary helium emissions. Rev. Sci. Instrum. **50**, 1047–1053, 1979

Dalgarno, A., McElroy, M.B., Stewart, A.I.: Electron impact excitation of the dayglow. J. Atmos. Sci. **26**, 753–762, 1969

Delaboudinière, J.P.: Possible contribution of radiation from the $2s2p^4\ ^2P$ level of OII in dayglow measurements of the HeI line at 584 Å. Planet. Space Sci. **25**, 193–195, 1977

Delaboudinière, J.P.: Multiple scattering effects in a cylindrical helium absorption cell operating close to the resonance line at λ584 Å. J. Quant. Spectrosc. Radiat. Transfer **22**, 411–434, 1979

Fahr, H.J., Shizgal, B.: Modern exospheric theories and their observational relevance. Rev. Geophys. Space Phys. **21**, 75–124, 1983

Fahr, H.J., Crifo, J.F., Wulf-Mathies, C., Seidl, P.: Daytime observations of helium 584 Å radiation by a rocket-borne resonance absorption cell. Astron. Astrophys. **58**, L21–L24, 1977

Feldman, P.D., Anderson, Jr., D.E., Meier, R.R., Gentieu, E.P.: The ultraviolet dayglow 4. The spectrum and excitation of singly ionized oxygen. J. Geophys. Res. **86**, 3583–3588, 1981

Gentieu, E.P., Feldman, P.D., Eastes, R.W., Christensen, A.B.: Spectroscopy of the extreme ultraviolet dayglow during

active solar conditions. Geophys. Res. Lett. **8**, 1242–1245, 1981

Gentieu, E.P., Feldman, P.D., Meier, R.R.: Spectroscopy of the extreme ultraviolet dayglow at 6.5 Å resolution: atomic and ionic emissions between 530 and 1240 Å. Geophys. Res. Lett. **6**, 325–328, 1979

Gledhill, J.A., Hoffman, R.A.: Nighttime observations of 0.2- to 26-keV electrons in the South Atlantic anomaly made by Atmosphere Explorer C. J. Geophys. Res. **86**, 6739–6744, 1981

Green, A.E.S., Barth, C.A.: Calculations of the photoelectron excitation of the dayglow. J. Geophys. Res. **72**, 3975–3986, 1967

Hedin, A.E., Salah, J.E., Evans, J.V., Reber, C.A., Newton, G.P., Spencer, N.W., Kayser, D.C., Alcaydé, D., Bauer, P., Cogger, L., McClure, J.P.: A global thermospheric model based on mass spectrometer and incoherent scatter data. MSIS 1. N_2 density and temperature. J. Geophys. Res. **82**, 2139–2147, 1977a

Hedin, A.E., Reber, C.A., Newton, G.P., Spencer, N.W., Brinton, H.C., Mayr, H.G., Potter, W.E.: A global thermospheric model based on mass spectrometer and incoherent scatter data. MSIS 2. Composition. J. Geophys. Res. **82**, 2148–2156, 1977b

Heroux, L., Higgins, J.E.: Summary of full-disk solar fluxes between 250 and 1940 Å. J. Geophys. Res. **82**, 3307–3310, 1977

Huffman, R.E., LeBlanc, F.J., Larrabee, J.C., Paulsen, D.E.: Satellite vacuum ultraviolet airglow and auroral observations. J. Geophys. Res. **85**, 2201–2215, 1980

Kumar, S., Bowyer, S., Lampton, M.: Observations of the Helium II 304-Å and Helium I 584-Å atmospheric dayglow radiation. J. Geophys. Res. **78**, 1107–1114, 1973

Landau, L.D., Lifshitz, E.M.: Theoretical Physics. New York: Pergamon Press 1964

Landolt-Börnstein: Zahlenwerte und Funktionen. 5. Teil Atomkerne und Elementarteilchen, 325–351. Berlin-Göttingen-Heidelberg: Springer-Verlag 1952

Lay, G., Fahr, H.J., Wulf-Mathies, C.: Spectrophotometric investigations of He-I/II resonance emissions with a rocket-borne multisensor resonance cell instrumentation. Proc. ESA Symp. on European Rocket/Balloon Research, Bournemouth (U.K.), 1980

Leinert, C., Klüppelberg, D.: Stray light suppression in optical space experiments. Applied Optics **13**, 556–564, 1974

Maloy, J.O., Carlson, R.W., Hartmann, U.G., Judge, D.L.: Measurement of the profile and intensity of the solar HeI λ 584-Å resonance line. J. Geophys. Res. **83**, 5685–5690, 1978

Marion, J.B. (ed.): Nuclear Physics. In: American Institute of Physics Handbook **8**-169ff., 1972

Meier, R.R., Strickland, D.J., Feldman, P.D., Gentieu, E.P.: The ultraviolet dayglow 1. Far UV emissions of N and N_2. J. Geophys. Res. **85**, 2177–2184, 1980

Meier, R.R., Weller, C.S.: EUV resonance radiation from helium atoms and ions in the geocorona. J. Geophys. Res. **77**, 1190–1204, 1972

Ogawa, T., Tohmatsu, T.: Sounding rocket observation of Helium 304- and 584-Å glow. J. Geophys. Res. **76**, 6136–6145, 1971

Paresce, F., Bowyer, S., Kumar, S.: Evidence for an interstellar or interplanetary source of diffuse HeI 584 Å radiation. Astrophys. J. **183**, L87–L90, 1973a

Paresce, F., Bowyer, S., Kumar, S.: Observations of the HeII 304 Å radiation in the night sky. J. Geophys. Res. **78**, 71–79, 1973b

Paresce, F., Fahr, H., Lay, G.: A search for interplanetary HeII, 304-Å emission. J. Geophys. Res. **86**, 10,038–10,048, 1981

Po Lee, Weissler, G.L.: Absorption cross section of helium and argon in the extreme ultraviolet. Phys. Rev. **99**, 540–542, 1955

Rawer, K., Ramakrishnan, S., Bilitza, D.: International Reference Ionosphere International Union of Radio Science (URSI), Brussels, 1978

Riegler, G.R., Garmire, G.P.: Observations of the extreme ultraviolet nightglow. J. Geophys. Res. **79**, 226–232, 1974

Sommerfeld, A.: Mathematische Theorie der Diffraction. Math. Ann. **47**, 317–391, 1896

Strickland, D.J., Donahue, T.M.: Excitation and radiative transport of OI 1304 Å resonance radiation I. The dayglow. Planet. Space Sci. **18**, 661–689, 1970

Thomas, G.E.: The interstellar wind and its influence on the interplanetary environment. Ann. Rev. Earth Planet. Sci. **6**, 173–204, 1978

Thomas, G.E., Anderson, Jr., D.E.: Global atomic hydrogen density derived from OGO-6 Lyman α measurements. Planet. Space Sci. **24**, 303–312, 1976

Vernov, S.N., Gorchakov, E.V., Shavrin, P.I., Sharvina, K.N.: Radiation belts in the region of the South-Atlantic magnetic anomaly. Space Sci. Rev. **7**, 490–533, 1967

Weller, C.S., Meier, R.R.: First satellite observations of the He^+ 304-Å radiation and its interpretation. J. Geophys. Res. **79**, 1572–1574, 1974

Received Oct. 19, 1983/Accepted Jan. 4, 1984